Atmos. Chem. Phys. Discuss., doi:10.5194/acp-2016-30, 2016
Manuscript under review for journal Atmos. Chem. Phys.
Published: 22 January 2016
© Author(s) 2016. CC-BY 3.0 License.

Atmospheric Chemistry and Physics Discussions

Global direct aerosol radiative forcing, as constrained by comprehensive observations

Chul E. Chung[1], Jung-Eun Chu[2], Yunha Lee[3], Twan van Noije[4], Hwayoung Jeoung[5], Kyung-Ja Ha[2], Marguerite Marks[6]
[1]Desert Research Institute, Reno, 89512, USA
[2]Pusan National University, Busan, 46241, Korea
[3]Washington State University, Pullman, 99164, USA
[4]Royal Netherlands Meteorological Institute, AE De Bilt, 3730, Netherlands
[5]National Meteorological Satellite Center, 27803, Korea
[6]Carnegie Mellon University, Pittsburgh, 15213, USA

Correspondence to: C. E. Chung (Eddy.Chung@dri.edu)

Abstract. Aerosols directly affect the radiative balance of the Earth through absorption and scattering of solar radiation. Although the contributions of absorption (heating) and scattering (cooling) of sunlight have proved difficult to quantify, the consensus is that anthropogenic aerosols cool the climate, partially offsetting the warming by rising greenhouse gas concentrations. Recent estimates of global direct aerosol radiative forcing are −0.35±0.5 Wm^{-2}, and these estimates depend either entirely or heavily on aerosol simulation. Here, we integrate a comprehensive suite of satellite and ground-based observations to constrain total AOD, its fine-mode fraction, the vertical distribution of aerosols and clouds, and the co-location of clouds and overlying aerosols. We find that fine-mode forcing is −0.46 Wm^{-2} (−0.54 ~ −0.39 Wm^{-2}). Fine-mode aerosols include sea salt and dust aerosols, and we find that these natural aerosols pose a very large cooling (−0.44 ~ −0.26 Wm^{-2}) when constrained by observations. When the contribution of these natural aerosols is subtracted from the fine-mode forcing, the net becomes −0.10 (−0.28 ~ +0.05) Wm^{-2}. The net forcing arises from carbonaceous, sulfate and nitrate aerosols. Despite uncertainties in the anthropogenic fraction of these aerosols, this −0.28 ~ +0.05 Wm^{-2} range compels the direct aerosol forcing to be near zero.

1. Introduction

Atmospheric aerosols absorb and scatter solar radiation and act as cloud condensation nuclei, thus affecting cloud albedo and lifetime. The climatic effect of aerosols is usually quantified in terms of radiative forcing, defined as the net radiative flux perturbation at the top of the atmosphere (TOA) owing to aerosol changes since pre-industrial time to the present. The magnitude of aerosol radiative forcing is recognized as the most uncertain component of estimated total radiative forcing (Myhre, 2013). The magnitude of the global aerosol direct radiative forcing (that due to absorption and scattering) has been estimated to range from −0.85 to + 0.15 Wm^{-2} (Myhre, 2013).

Direct aerosol forcing has been commonly estimated by a model-based approach of simulating global aerosol amount, distribution, and characteristics, and processing the predicted global aerosol distribution by a radiation model. Global aerosol simulations are subject to large uncertainties in emissions, transport, gas-to-aerosol

Atmos. Chem. Phys. Discuss., doi:10.5194/acp-2016-30, 2016
Manuscript under review for journal Atmos. Chem. Phys.
Published: 22 January 2016
© Author(s) 2016. CC-BY 3.0 License.

Atmospheric Chemistry and Physics Discussions

conversion, aerosol aging, aerosol mixing state, and wet and dry deposition (Bond et al., 2004; Ma et al., 2012). The large spread among direct aerosol forcing estimates (Myhre, 2013) is attributable largely to these simulation uncertainties. Attempts have been made to constrain global aerosol simulations by observations (Chung et al., 2005; Bellouin et al., 2008; Myhre, 2009; Su et al., 2013) but these semi-empirical studies are not sufficient to validate the model based estimates given heavy model dependence. In particular, the anthropogenic fraction of aerosol amount was obtained from aerosol simulations (Chung et al., 2005; Myhre, 2009; Su et al., 2013) or by utilizing the fine-mode fraction (FMF) of satellite-derived AOD (Aerosol Optical Depth) over ocean (Bellouin et al., 2008; Chung et al., 2005). Over the land, where most anthropogenic aerosols are located, no study constrained the anthropogenic fraction by observations yet.

In this study, we provide observational estimates of direct aerosol radiative forcing. Here, we constrain total AOD, the single scattering albedo (SSA), and the asymmetry parameter by observations as in previous semi-empirical studies (Chung et al., 2005; Myhre, 2009; Su et al., 2013). In addition, we use observations to constrain the aerosol vertical profile, and the FMF of AOD over land as well as ocean. Atmospheric aerosols consist of carbonaceous, sulfate, nitrate, sea salt and dust aerosols. The first three types of aerosols are fine-mode particles which are mostly anthropogenic while a sizable portion of sea salt and dust aerosols are also in the fine mode. Thus, using observations to derive fine-mode AOD over the globe is an important advance but is not quite sufficient to accurately quantify anthropogenic AOD. In the present study, we will use observations to constrain the fine-mode sea salt and dust AODs, and subtract this component from the total fine-mode AOD. The goal of this study is to provide the most observational estimate of direct aerosol radiative forcing to date.

2. Data

All the datasets used in this study are monthly means.

2.1 Global observational data

AOD is a common measure of aerosol amount. AERONET (Aerosol Robotic Network; Holben et al., 1998) AOD is known to be the most accurate global-scale product. However, AERONET sites are non-uniformly distributed over the globe while less-reliable satellite (MODIS and MISR) AODs have nearly full global coverage. We follow the approach of Lee and Chung (2013) in nudging or adjusting the satellite AOD towards AERONET AOD to construct globally-reliable AOD. Fig. 1A shows this adjusted AOD.

AOD at 550 nm, fine-mode AOD (fAOD) at 500 nm, and coarse-mode AOD at 500 nm from 2001 to 2010 are obtained by the approach in Lee and Chung (2013), except that instead of directly using the monthly AERONET FMF data we used the monthly AERONET fAOD (from the direct sun measurements and the Spectral Deconvolution Algorithm as in Lee and Chung) and total AOD to derive the FMF. Like in Lee and Chung (2013), we nudged MODIS and MISR data towards AERONET data to derive reliable fine-mode AOD over the globe.

Atmos. Chem. Phys. Discuss., doi:10.5194/acp-2016-30, 2016
Manuscript under review for journal Atmos. Chem. Phys.
Published: 22 January 2016
© Author(s) 2016. CC-BY 3.0 License.

Atmospheric Chemistry and Physics Discussions

We computed the 2001-2010 average for each calendar month at the T42 resolution. In these datasets, the data gaps are filled by the GOCART simulation (Chin et al., 2002) as in Lee and Chung (2013). These data gaps are predominantly confined to the polar regions, and are even fewer in polar summer.

We obtain fAOD at 550 nm by subtracting coarse-mode AOD at 500 nm from AOD at 550 nm, assuming that coarse-mode AOD does not change from 500 nm to 550 nm.

2.2 Global semi-observational data

To compute the direct aerosol radiative effect, aerosol optical characteristics, such as SSA (Single Scattering Albedo), must be specified. We construct a global distribution of SSA by nudging global model-simulated (Chin et al., 2002) SSA towards AERONET SSA.

550 nm SSA, 550 nm ASY (Asymmetry Parameter), CA_AE (Co-albedo Å ngström Exponent; Co-albedo = 1-SSA) for total (natural + anthropogenic) aerosols are obtained by combining the GOCART simulation (Chin et al., 2002) and AERONET data. The GOCART simulation is nudged towards the AERONET data. Specifically, for ASY and CA_AE the following nudging equation is used:

$$N_ASY_j = G_ASY_j \times \frac{\sum_i \frac{AERONET_{j,i} - G_ASY_{j,i}}{d_{j,i}^4}}{\sum_i \frac{1}{d_{j,i}^4}}$$

where N_ASY_j is the adjusted new value of ASY at grid j; $AERONET_{j,i}$ is an AERONET ASY at station location i near grid j; $d_{j,i}$ is the distance between j and i; and $G_ASY_{j,i}$ is the GOCART ASY at the grid box containing $AERONET_{j,i}$. Here the AERONET data and the GOCART simulation are on the T42 grids.

For SSA, the following equation is used:

$$(1-N_SSA_j) = (1 - G_SSA_j) \times \frac{\sum_i \frac{1-AERONET_{j,i}}{d_{j,i}^4}}{\sum_i \frac{1-G_SSA_{j,i}}{d_{j,i}^4}} \quad .$$

Another way to interpret the above equations is that the GOCART simulation is an interpolation tool. The equation for SSA differs from that for ASY or CA_AE, because SSA cannot be negative, and its value starts from 1.0. The above equations are applied for each grid and each calendar month. The final values are the simulation nudged towards AERONET values.

Before combining the GOCART simulation and AERONET data, the 2001-2010 average was calculated from the monthly Level 2.0 AERONET data for each calendar month. The average of the AERONET SSA or ASY was AOD-weighted. Then, SSA and ASY at 550 nm were obtained from the neighboring wavelength values through linear interpolation. AERONET CA_AE was obtained by the 2001-2010 SSA averages at 440, 675 and 870 nm for each calendar month. Please note that AERONET only gives level 2 quality SSA when AOD at 440 nm >0.4, and therefore many regions of the earth do not have AERONET SSA data.

The products from combining the GOCART simulation and AERONET data are semi-observational and we address the model dependence as follows.

Atmos. Chem. Phys. Discuss., doi:10.5194/acp-2016-30, 2016
Manuscript under review for journal Atmos. Chem. Phys.
Published: 22 January 2016
© Author(s) 2016. CC-BY 3.0 License.

Atmospheric Chemistry and Physics Discussions

SSA, apart from AOD, is the most influential parameter in aerosol direct forcing (Chung, 2012). We generated three different sets of simulated SSA:

SSA1 = (0.19×BC+0.85×OA+1.0×sulfate+1.0×sea-salt+0.96×dust)/total_AOD;

SSA2 = (0.14×BC+0.8×OA+1.0×sulfate+1.0×sea-salt+0.96×dust)/total_AOD; and

SSA3 = (0.19×BC+0.98×OA+1.0×sulfate+1.0×sea-salt+0.96×dust)/total_AOD.

BC above refers to the GOCART BC AOD at 550 nm. The above three sets of simulated SSA may not fully represent the uncertainty in simulated SSA. Thus, in SSA2 (more absorbing case), we even doubled the magnitude of BC AOD (given a large uncertainty in simulated BC amount). Then, we nudged the 3 sets of simulated SSA towards the same AERONET SSA, which gave 3 sets of semi-observational SSA. Finally, we computed the average, maximum and minimum SSAs from the three sets of SSA over each grid and each calendar month, and then re-generated three sets of SSA (average: baseline; maximum; and minimum; see Fig. 2). This re-generation increases the global-average SSA difference between the least absorbing and most absorbing cases. We do this re-generation in an attempt to fully bracket the simulated SSA uncertainty.

Simulated ASY at 550 nm and CA_AE are computed as follows.

ASY = (0.6×CA+0.7×sulfate+0.75×sea-salt+0.75×dust)/total_SAOD. CA here refers to Carbonaceous Aerosol (i.e., BC+OA) SAOD (Scattering AOD) at 550 nm from GOCART.

CA_AE = (-0.53×CA+2.215×dust)/total_AOD, where CA refers to CA AOD. These simulations were nudged towards AERONET data as explained earlier. We do not address the model dependence on ASY or CA_AE, since its impact on aerosol forcing is tiny compared to the impact of SSA uncertainty. To be sure, we re-generated the ASY using doubled BC AOD while holding other components (such as SSA) fixed, and found that the global direct aerosol effect changes by less than 0.002 Wm^{-2}.

The GOCART simulations were prepared as follows. We used sea salt AOD from Chin et al. (Chin et al., 2002), and BC (black carbon), OA (Organic Aerosol), dust and sulfate AODs from the Giovanni website (http://gdata1.sci.gsfc.nasa.gov/daac-bin/G3/gui.cgi?instance_id=neespi), which contains GOCART model output from 2000 to 2007. These AODs are monthly means at 550 nm. Then, the climatological seasonal cycle for the available data period was computed. We used these simulated AOD values to compute the simulated SSA, ASY and CA_AE.

2.3 Global simulations

For coarse-mode aerosols, we assumed ASY to be 0.75 and AE (Å ngström Exponent for AOD) to be 0.0. For 550 nm SSA and CA_AE, we rely entirely on the GOCART simulations as follows: SSA = (1.0×sea-salt+0.96×dust)/lAOD, where dust refers to GOCART dust AOD and lAOD refers to GOCART dust and sea salt AODs combined. CA_AE=2.215×dust/lAOD. Although we rely entirely on simulated SSA for coarse-mode aerosols, we find very small the coarse-mode forcing uncertainty resulting from simulated SSA. For instance, when we change the amount of dust by 35%, the difference in coarse-mode aerosol forcing is only 0.01 Wm^{-2}.

Atmos. Chem. Phys. Discuss., doi:10.5194/acp-2016-30, 2016
Manuscript under review for journal Atmos. Chem. Phys.
Published: 22 January 2016
© Author(s) 2016. CC-BY 3.0 License.

Atmospheric Chemistry and Physics Discussions

For fine-mode sea salt and dust aerosols, we assumed ASY to be 0.6 and AE to be 1.85. For 550 nm SSA and CA_AE, we rely entirely on simulated fAODs as follows: SSA = (1.0×sea-salt+0.96×dust)/fAOD, where dust refers to dust fAOD and fAOD refers to dust and sea salt fAODs combined. CA_AE=2.215×dust/lAOD.

These simulated aerosol optical properties were used in the MACR model runs, leading to the results in Table 1.

2.4 Vertical profile

Aerosol vertical profiles are obtained from the space-borne CALIOP lidar (Liu et al., 2009). To construct the profile, we used the daytime CALIPSO lidar level 2.0 data (Liu et al., 2009) from June 2006 to Oct. 2011. We processed the level 2.0 data, and obtained clear-sky aerosol extinction coefficient at 532 nm at the T42 spatial resolution and 500 m MACR model vertical resolution. We filled the data gaps using available neighboring data through linear interpolation. We then computed the climatological seasonal cycle for the entire available data period. Over some grids and calendar months, the aerosol extinction coefficient has extremely low magnitudes, in which case, the PBL profile as in Chung et al. (Chung et al., 2012) is applied. The threshold for applying the PBL profile is a vertically-summed aerosol extinction coefficient of 0.03. Note that a vertically-summed aerosol extinction coefficient of 0.03 is associated with a very small amount of aerosol and the effect of these aerosols on global aerosol forcing is very small. Also note that the aerosol vertical profile from CALIPSO is scaled to match the AOD observations obtained by integrating AERONET, MODIS and MISR data (as shown in Fig. 1A) since the latter observations describe clear-sky AOD too and give better accuracy. The clear-sky aerosol profile from CALIPSO is assumed to be applied to an entire T42 grid in the MACR model.

To adjust the magnitude of AOD over cloud by CALIPSO data, we use the daytime CALIPSO lidar level 3.0 data (Winker et al., 2013), which are globally-gridded (5° x 2°) monthly mean data spanning from June 2006 to Jan. 2012. Specifically, we use the CALIPSO level 3.0 derived ratio of clear-sky AOD to above-cloud AOD to modify the aerosol amount over cloud over each grid cell in the MACR model. The level 3.0 data have gaps. Again, the data gaps were filled using a linear interpolation, then the data was converted into the T42 grids, and the climatological seasonal cycle was obtained before the use in MACR model.

For coarse-mode aerosols, we apply the same profiles given a lack of observations. Because coarse-mode aerosols are not very absorbing, the effect of the vertical profile is very small (Choi and Chung, 2014).

3. Radiation model

We use the Monte-Carlo Aerosol Cloud Radiation (MACR) model as in Choi and Chung (Choi and Chung, 2014), except that we improved the low cloud height in the model using the CALIPSO level 2.0 data. As in Choi and Chung (Choi and Chung, 2014), the height of low cloud bottom is set to 750 m above the ground. The low cloud top height is set to 1250 m, when the maximum low cloud height over a 5° x 2° grid (and during a whole month) from CALIPSO data is 750m ~ 1750m. When the CALIPSO maximum low cloud height exceeds 1750 m, the low cloud top height in the model is set to 1750 above the ground).

Atmos. Chem. Phys. Discuss., doi:10.5194/acp-2016-30, 2016
Manuscript under review for journal Atmos. Chem. Phys.
Published: 22 January 2016
© Author(s) 2016. CC-BY 3.0 License.

Atmospheric Chemistry and Physics Discussions

This model, which accounts for multi-layer clouds from satellite observations, has undergone comprehensive validation of the simulated fluxes at the TOA and at the surface over 100 land and island stations (agreement with observations is within a few Wm^{-2}) (Kim and Ramanathan, 2008). Only short-wave radiation is considered.

4. Aerosol direct radiative effect

We first address the direct aerosol radiative effect (forcing due to natural and anthropogenic aerosols). We incorporated the integrated global aerosol data (as explained in section 2) into the MACR model. Fig. 1B shows the direct aerosol radiative effect as estimated by the MACR model. The direct aerosol radiative effect in Fig. 1B also incorporates that aerosol amount over cloud might differ from that at the same height in clear skies in the same region. The CALIOP lidar is able to retrieve aerosol amount over cloud as well as in clear skies, and so we used this lidar data to constrain the aerosol amount over cloud (as explained in section 2.4). This procedure could be important since radiation modeling studies showed that the sensitivity of aerosol forcing to the aerosol vertical profile arises mainly as a consequence of the location of absorbing particles relative to cloud (Choi and Chung, 2014). On the other hand, cloud is brighter than most surfaces during daytime, and this could create a low bias in aerosol amount over cloud, as retrieved by the CALIOP lidar (Chepfer et al., 2013; Hunt et al., 2009; Kacenelenbogen et al., 2014; Vaughan and coauthors, 2009). To be sure, we re-computed the aerosol radiative effect assuming equal amounts between clear skies and over cloud, and found that the forcing only increases by 0.03 Wm^{-2} in global average.

Next, we estimate fine-mode aerosol forcing. Since the FMF of aerosols over land is difficult to accurately retrieve from satellites, past semi-empirical estimates (Bellouin et al., 2008; Myhre, 2009) only used the FMF of AOD from satellite observations over the ocean. In contrast, AERONET data provide relatively reliable FMF over both land and ocean (with the AERONET data being predominantly over land). Following the approach of Lee and Chung (Lee and Chung, 2013) satellite data are nudged toward AERONET data to construct global FMF and thus fine-mode AOD (see section 2.1 for details). Fig. 3A shows this fine-mode AOD, which, as expected, is largest over industrial and biomass burning areas.

Fig. 3B shows the estimated fine-mode direct radiative forcing as the difference between the coarse-mode and total (coarse + fine modes) aerosol radiative effect. Fine-mode direct forcing is negative almost everywhere, except over the eastern equatorial Atlantic, the Sahara, and the Arabian Desert. These areas of positive forcing result from highly absorbing particles above highly reflective surfaces or low cloud. The global average of the fine-mode direct forcing is estimated as -0.46 Wm^{-2}. In this computation, aerosol simulation using GOCART was used to provide interpolation for aerosol optical characteristics, such as SSA. To quantify uncertainty in the model dependence, two sets of additional simulations were conducted, representing lower and upper limits of absorption (see section 2.2 and Fig. 2). Fine-mode direct forcing is estimated to range between -0.54 Wm^{-2} and -0.39 Wm^{-2},

Atmos. Chem. Phys. Discuss., doi:10.5194/acp-2016-30, 2016
Manuscript under review for journal Atmos. Chem. Phys.
Published: 22 January 2016
© Author(s) 2016. CC-BY 3.0 License.

Atmospheric Chemistry and Physics Discussions

corresponding to these two limits (Table 1). Aerosol simulations yielding fine-mode forcing outside of the −0.54 ~ −0.39 Wm^{-2} range can be considered as inconsistent with observational constraints.

5. Fine-mode fraction (FMF) of sea salt and dust AODs

The fine-mode direct radiative forcing estimate, as shown in Fig. 3B, includes the contribution from natural fine-mode sea salt and dust aerosols. To subtract this contribution from the fine-mode direct radiative forcing estimate, we address the FMF of sea salt and dust AODs here. Instead of using simulated fine-mode sea salt and dust AOD (and thus being 100% subject to model uncertainties), we use observed coarse-mode AOD × $\frac{\text{SD_FMF}}{1-\text{SD_FMF}}$, where SD_FMF refers to the simulated FMF of sea salt + dust AOD. An underlying assumption therein is that coarse-mode AOD results only from sea salt and dust aerosols. We obtain the observed coarse-mode AOD by subtracting fine-mode AOD from total AOD where the fine-mode and total AODs were obtained by integrating AERONET, MODIS and MISR data (see section 2.1).

For simulated FMF, we used AOD (at 550 nm) simulations from GOCART, the Spectral Radiation-Transport Model for Aerosol Species (SPRINTARS), the Tracer Model 5 (TM5) and ModelE2-TOMAS (briefly ModelE2 here). The SPRINTARTS output is from the AeroCom (Aerosol Comparisons between Observations and Models) Phase II (Schulz et al., 2009) hindcast experiments and the TM5 outputs are from the AeroCom Phase III. The ModelE2-TOMAS simulation was performed using the TwO-Moment Aerosol Sectional (TOMAS) microphysics module incorporated into the state-of-the-art general circulation model GISS ModelE2 (Lee et al., 2015). TOMAS module represents aerosol size distribution in many size categories or "bins" covering 10nm to 10μm. We used a Fast-TOMAS module (Lee and Adams, 2012) with a 15 bin version here, since Fast TOMAS reduces the computational burden by 2-3 times while well preserving the capability of computing fine-mode fraction compared to the original TOMAS model with 30 bins. The fine-mode fraction of dust and sea-salt aerosols from ModelE2-TOMAS was calculated by converting the mass output to AODs, and then applying the Spectral Deconvolution Algorithm (SDA) used in AERONET retrievals (O'Neill et al., 2003) to the AODs in order to create FMF consistent with AERONET FMF. A Mie-scattering code was used to compute size-resolved AOD at 380, 440, 500, 675 and 870 nm. Refractive indices for dust and sea-salt are taken from Optical Properties of Aerosol and Clouds (OPAC) dataset (Hess et al., 1998). The ModelE2-TOMAS simulation was nudged with wind from MERRA (Mordern Era Retrospective-analysis for Research and Applications) reanalysis from 2003 to 2005 after 3 years of spin-up. The simulation period for ModelE2-TOMAS is 2003-2005, and that for TM5, SPRINTARS and GOCART are 2001-2010, 2001-2008, and 2000-2007, respectively. Climatological AODs for each of 4 models were obtained by computing the average over the aforementioned simulation period for each calendar month.

Fig. 4 is displayed to compare various simulated FMFs with the observed FMF. First, we assess which simulation performs the best in simulating dust FMF by looking at the simulated FMFs (including FMF of non-dust particles) over dust dominated places where we use AERONET observations to validate the simulated FMFs. Dust-dominated AERONET sites in Fig. 4A were selected with the following criteria: 550 nm FMF < 0.3, AAE

Atmos. Chem. Phys. Discuss., doi:10.5194/acp-2016-30, 2016
Manuscript under review for journal Atmos. Chem. Phys.
Published: 22 January 2016
© Author(s) 2016. CC-BY 3.0 License.

Atmospheric Chemistry and Physics Discussions

(Absorption Ångström Exponent) > 2.0 and 550 nm AAOD (Absorption AOD) > 0.03. We again followed the approach by Lee and Chung (Lee and Chung, 2013) in computing AERONET FMF, AAE and AAOD. Please note that in Fig. 4 we used climatological means for each calendar month; again for FMF we used mean AODs to compute the FMF instead of averaging FMFs. Fig. 4B suggests that models tend to over-estimate dust FMF, at least over dust-dominated places.

Regarding sea salt FMF, we look at the simulated sea salt FMFs and observed total FMF over relatively pristine oceans (Fig. 4C). Organic and sulfate aerosols can be over remote oceans (Shank et al., 2012) in addition to fine-mode sea salt. Fig. 4C shows large disagreements between sea salt FMF simulations, where one of the models (Chin et al., 2002) clearly overestimates sea salt FMF given that the simulated sea salt FMF is near the total FMF from observations. In view of this, we scale down the simulated fine-mode dust FMF and mix sea salt FMF simulations to calculate FMF of sea salt.

We scale down the simulated dust FMF and mix sea salt FMF simulations by having multiple estimates (best estimate and sensitivity runs) to address the uncertainty in simulated FMF. The FMF of sea salt + dust AOD for our best estimate (i.e., baseline) is prepared using ModelE2 as follows. We scale up the coarse-mode dust AOD by 1.16 times and scale down the fine-mode dust AOD by 0.56 times so that ModelE2 would match AERONET in FMF and AOD over dust-dominated sites. We scale down sea salt AOD (both fine and coarse modes) by 0.6 times so that the total AOD from ModelE2 matches AERONET data over sea salt dominated sites. We use ModelE2 for the best estimate since this model has an advanced size distribution description and uses the SDA to divide the AOD into fine-mode and coarse-mode components. For sensitivity run 1, we replace the ModelE2 dust AOD by the GOCART dust AOD where the coarse-mode dust AOD is scaled up by 1.3 times and the fine-mode dust AOD is scaled down by 0.74 times. For sensitivity run 2, we use the baseline set-up except that for sea salt AOD we equally mix the outputs from GOCART, TM5 and ModelE2.

6. Implications for global direct aerosol radiative forcing

We estimate the forcing due to fine-mode sea salt and dust aerosols at −0.35 (−0.44 ~ −0.26) Wm^{-2} (Table 1). In those studies where these aerosols were assumed to be negligible, the aerosol direct forcing estimates would have been that much more negative than in reality. When we remove the contribution of these aerosols from the fine-mode forcing, we end up with aerosol forcing due to carbonaceous, sulfate and nitrate aerosols (anthropogenic + natural). As Fig. 6A shows, this net forcing is large and positive over Africa and the downstream areas where biomass burning is the major source. The forcing is also conspicuously positive over the Sahara, probably because biomass burning aerosols in the Sahel are advected northwards (Haywood et al., 2008) and bright desert surfaces turn the forcing positive. Fig. 6B shows that these advected aerosols have a relatively small forcing in the atmosphere due to smaller aerosol amounts. Outside of Africa and the downstream areas, the forcing is a mixture of positive and negative values, and negative values slightly outweigh positive values. The global average (including Africa) is −0.10 Wm^{-2} with an uncertainty range of −0.54+0.26 ~ −0.39+0.44 (i.e., −0.28~+0.05).

Atmos. Chem. Phys. Discuss., doi:10.5194/acp-2016-30, 2016
Manuscript under review for journal Atmos. Chem. Phys.
Published: 22 January 2016
© Author(s) 2016. CC-BY 3.0 License.

Atmospheric Chemistry and Physics Discussions

The anthropogenic fraction (or pre-industrial fraction) of carbonaceous, sulfate and nitrate aerosols is uncertain. Black carbon, the only warming aerosol species in carbonaceous aerosol (black carbon + organic aerosol), sulfate and nitrate, is known to be mostly anthropogenic (Bond et al., 2011), which means that aerosol direct forcing is at least > −0.28 Wm^{-2}. Thus, we posit that aerosol direct forcing is less negative than the consensus, and likely near zero. This conclusion is consistent with the recent findings (Bahadur et al., 2012; Chung et al., 2012) that observationally-constrained black carbon forcing is more positive than currently simulated, and organic aerosols are more absorbing than currently treated.

Our observational approach makes the results subject to observation errors. AERONET SSA, in particular, is subject to potentially significant uncertainties due to various assumptions used in the retrieval algorithms. Thus, the uncertainty in our estimates of fine-mode forcing, e.g., might be larger than −0.54 ~ −0.39 Wm^{-2}. However, studies (Eck et al., 2010; Leahy et al., 2007) showed that AERONET SSA is higher or lower than in-situ measurements depending on location, season, in-situ measurement device, etc. Furthermore, in-situ measurements are also subject to uncertainties, and so the difference between the AERONET SSA and in-situ measured SSA is not necessarily due only to the AERONET data error. Overall, we believe that AERONET observations likely have smaller biases and provide more credible results than aerosol simulations. At least, our observational approach offers an independent estimate than aerosol simulations.

Acknowledgment

The authors are thankful to P. Adams of Carnegie Mellon University and N.T. O'Neill at Canadian Network for the Detection of Atmospheric Change for valuable inputs. This study was funded by the National Science Foundation (AGS-1455759).

Atmos. Chem. Phys. Discuss., doi:10.5194/acp-2016-30, 2016
Manuscript under review for journal Atmos. Chem. Phys.
Published: 22 January 2016
© Author(s) 2016. CC-BY 3.0 License.

Atmospheric Chemistry and Physics Discussions

References

Bahadur, R., Praveen, P. S., Xu, Y., and Ramanathan, V.: Solar absorption by elemental and brown carbon determined from spectral observations, Proceedings of the National Academy of Sciences, 109, 17366-17371, 2012.

Bellouin, N., Jones, A., Haywood, J., and Christopher, S. A.: Updated estimate of aerosol direct radiative forcing from satellite observations and comparison against the Hadley Centre climate model, Journal of Geophysical Research: Atmospheres, 113, n/a-n/a, 2008.

Bond, T. C., Streets, D. G., Yarber, K. F., Nelson, S. M., Woo, J.-H., and Klimont, Z.: A technology-based global inventory of black and organic carbon emissions from combustion, J. Geophys. Res., 109, D14203, 2004.

Bond, T. C., Zarzycki, C., Flanner, M. G., and Koch, D. M.: Quantifying immediate radiative forcing by black carbon and organic matter with the Specific Forcing Pulse, Atmos. Chem. Phys., 11, 1505-1525, 2011.

Chepfer, A., Cesana, G., Winker, M. A., Getzewich, B., Vaughan, K. A., and Liu, Z.: Comparison of two different cloud climatologies derived from CALIOP-attenuated backscattered measurements (Level 1): The CALIPSO-ST and the CALIPSO-GOCCP, Journal of Atmospheric and Oceanic Technology, 30, 725–744, 2013.

Chin, M., Ginoux, P., Kinne, S., Torres, O., Holben, B. N., Duncan, B. N., Martin, R. V., Logan, J. A., Higurashi, A., and Nakajima, T.: Tropospheric aerosol optical thickness from the GOCART model and comparisons with satellite and sun photometer measurements, J. Atmos. Sci., 59, 461-483, 2002.

Choi, J.-O. and Chung, C. E.: Sensitivity of aerosol direct radiative forcing to aerosol vertical profile, Tellus B, 66, 2014.

Chung, C. E., Ramanathan, V., and Decremer, D.: Observationally constrained estimates of carbonaceous aerosol radiative forcing, Proceedings of the National Academy of Sciences, 109, 11624-11629, 2012.

Chung, C. E., Ramanathan, V., Kim, D., and Podgorny, I. A.: Global anthropogenic aerosol direct forcing derived from satellite and ground-based observations, J. Geophys. Res., 110, D24207, 2005.

Chung, C. E.: Aerosol Direct Radiative Forcing: A Review, 2012.

Eck, T. F., Holben, B. N., Sinyuk, A., Pinker, R. T., Goloub, P., Chen, H., Chatenet, B., Li, Z., Singh, R. P., Tripathi, S. N., Reid, J. S., Giles, D. M., Dubovik, O., O'Neill, N. T., Smirnov, A., Wang, P., and Xia, X.: Climatological aspects of the optical properties of fine/coarse mode aerosol mixtures, J. Geophys. Res., 115, D19205, 2010.

Haywood, J. M. and Coauthors: Overview of the Dust and Biomass-burning Experiment and African Monsoon Multidisciplinary Analysis Special Observing Period-0, Journal of Geophysical Research D: Atmospheres, 113, 2008.

Hess, M., Koepke, P., and Schult, I.: Optical Properties of Aerosols and Clouds: The Software Package OPAC, B. Am. Meteorol. Soc., 79, 831-844, 1998.

Holben, B. N. and Coauthors: AERONET – A federated instrument network and data archive for aerosol characterization, Remote Sensing Environment, 66, 1-16, 1998.

Hunt, W. H., Winker, M. A., Vaughan, K. A., Powell, K. A., Lucker, P. L., and Weimer, C.: CALIPSO Lidar description and performance assessment, Journal of Atmospheric and Oceanic Technology, 26, 1214-1228, 2009.

Atmos. Chem. Phys. Discuss., doi:10.5194/acp-2016-30, 2016
Manuscript under review for journal Atmos. Chem. Phys.
Published: 22 January 2016
© Author(s) 2016. CC-BY 3.0 License.

Kacenelenbogen, M. S. and Coauthors: An evaluation of CALIOP/CALIPSO's aerosol-above-cloud (AAC) detection and retrieval capability, Journal of Geophysical Research D: Atmospheres, 119, 230-244, 2014.

Kim, D. and Ramanathan, V.: Solar radiation budget and radiative forcing due to aerosols and clouds, J. Geophys. Res., 113, D02203, 2008.

Leahy, L. V., Anderson, T. L., Eck, T. F., and Bergstrom, R. W.: A synthesis of single scattering albedo of biomass burning aerosol over southern Africa during SAFARI 2000, Geophys. Res. Lett., 34, L12814, 2007.

Lee, K. and Chung, C. E.: Observationally-constrained estimates of global fine-mode AOD, Atmospheric Chemistry and Physics, 13, 2907-2921, 2013.

Lee, Y. H. and Adams, P. J.: A Fast and Efficient Version of the TwO-Moment Aerosol Sectional (TOMAS) Global Aerosol Microphysics Model, Aerosol Science and Technology, 46, 678-689, 2012.

Lee, Y. H., Adams, P. J., and Shindell, D. T.: Evaluation of the global aerosol microphysical ModelE2-TOMAS model against satellite and ground-based observations, Geoscientific Model Development, 8, 631-667, 2015.

Liu, Z. and Coauthors: The CALIPSO Lidar Cloud and Aerosol Discrimination: Version 2 Algorithm and Initial Assessment of Performance, Journal of Atmospheric and Oceanic Technology, 26, 1198-1213, 2009.

Ma, X., Yu, F., and Luo, G.: Aerosol direct radiative forcing based on GEOS-Chem-APM and uncertainties, Atmos. Chem. Phys., 12, 5563-5581, 2012.

Myhre, G., D. Shindell, et al.: Anthropogenic and Natural Radiative Forcing. In: Climate Change 2013: The Physical Science Basis. Contribution of Working Group I to the Fifth Assessment Report of the Intergovernmental Panel on Climate Change, IPCC report, V, 2013.

Myhre, G.: Consistency between satellite-derived and modeled estimates of the direct aerosol effect, Science, 325, 187-190, 2009.

O'Neill, J. T., Eck, T. F., Smirnov, A., Holben, B. N., and Thulasiraman, S.: Spectral discrimination of coarse and fine mode optical depth, Journal of Geophysical Research D: Atmospheres, 108, 2003.

Schulz, M., Chin, M., and Kinne, S.: The aerosol model comparison project, AeroCom, phase II: clearing up diversity, IGAC Newsletter, 2009. 2009.

Shank, L. M., Howell, S., Clarke, A. D., Freitag, S., Brekhovskikh, V., Kapustin, V., McNaughton, C., Campos, T., and Wood, R.: Organic matter and non-refractory aerosol over the remote Southeast Pacific: Oceanic and combustion sources, Atmospheric Chemistry and Physics, 12, 557-576, 2012.

Su, W., Loeb, N. G., Schuster, G. L., Chin, M., and Rose, F. G.: Global all-sky shortwave direct radiative forcing of anthropogenic aerosols from combined satellite observations and GOCART simulations, Journal of Geophysical Research D: Atmospheres, 118, 655-669, 2013.

Vaughan, M. A. and coauthors: Fully automated detection of cloud and aerosol layers in the calipso lidar measurements, Journal of Atmospheric and Oceanic Technology, 26, 2034-2050, 2009.

Winker, D. M., Tackett, J. L., Getzewich, B. J., Liu, Z., Vaughan, M. A., and Rogers, R. R.: The global 3-D distribution of tropospheric aerosols as characterized by CALIOP, Atmos. Chem. Phys., 13, 3345-3361, 2013.

Atmos. Chem. Phys. Discuss., doi:10.5194/acp-2016-30, 2016
Manuscript under review for journal Atmos. Chem. Phys.
Published: 22 January 2016
© Author(s) 2016. CC-BY 3.0 License.

Atmospheric Chemistry and Physics Discussions

Tables

Aerosol direct forcing	TOA (in Wm^{-2})	Atmosphere	Surface
Direct aerosol radiative effect	-2.28	+4.77	-7.05
Fine-mode forcing (baseline)	-0.46	+3.88	-4.33
Fine-mode forcing (sensitivity run 1: least absorbing case)	-0.54	+3.63	-4.17
Fine-mode forcing (sensitivity run 2: Most absorbing case)	-0.39	+4.08	-4.47
Fine-mode sea salt and dust forcing (baseline: ModelE2 with reduced dust FMF)	-0.35	+0.24	-0.59
Fine-mode sea salt and dust forcing (sensitivity run 1: reduced GOCART dust FMF + ModelE2 sea salt FMF)	-0.26	+0.16	-0.42
Fine-mode sea salt and dust forcing (sensitivity run 2: Reduced ModelE2 dust FMF + ModelE2/GOCART/TM5 mix sea salt FMF)	-0.44	+0.27	-0.71
Fine-mode forcing without dust and sea salt (baseline)	-0.10	+3.64	-3.74

Table 1. Global 2001-2010 average of aerosol radiative forcing calculated with the MACR model.

Atmos. Chem. Phys. Discuss., doi:10.5194/acp-2016-30, 2016
Manuscript under review for journal Atmos. Chem. Phys.
Published: 22 January 2016
© Author(s) 2016. CC-BY 3.0 License.

Atmospheric Chemistry and Physics Discussions

Figures

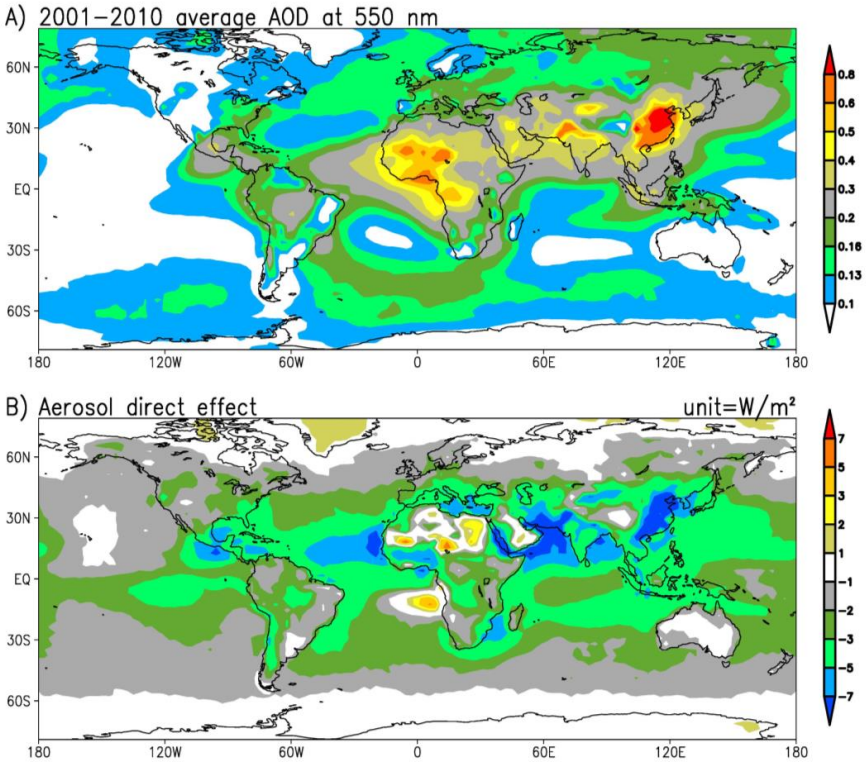

Figure 1. A) 2001-2010 mean 550 nm AOD obtained by integrating MODIS, MISR and AERONET AOD. B) 2001-2010 mean direct aerosol radiative effect. This estimate includes natural aerosols.

Atmos. Chem. Phys. Discuss., doi:10.5194/acp-2016-30, 2016
Manuscript under review for journal Atmos. Chem. Phys.
Published: 22 January 2016
© Author(s) 2016. CC-BY 3.0 License.

Atmospheric Chemistry and Physics Discussions

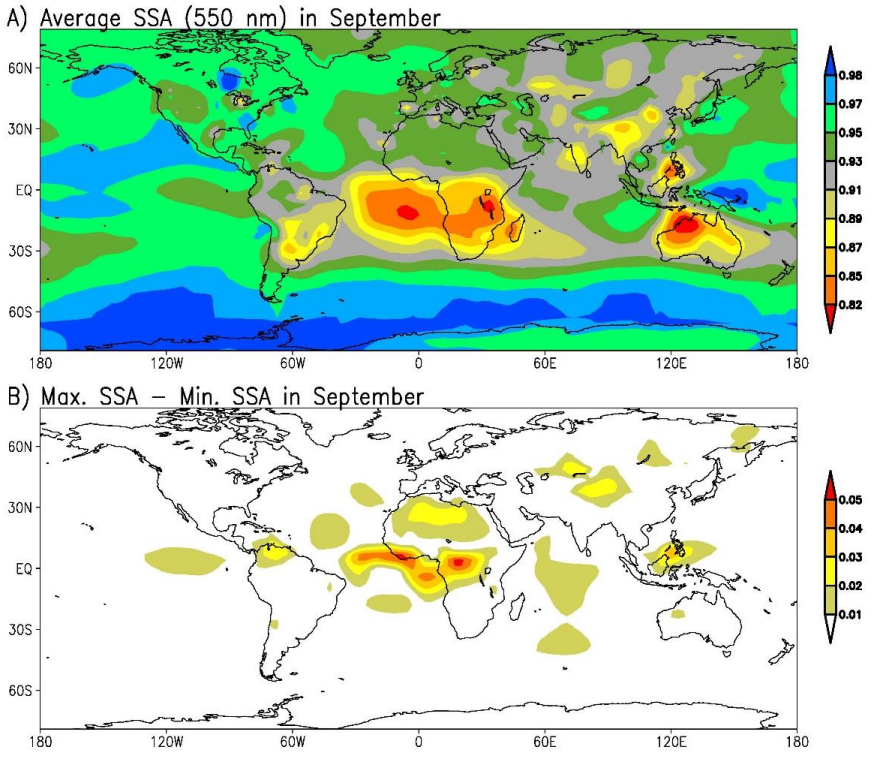

Figure 2. Integration of simulated SSA and AERONET SSA. A) Average SSA. B) Maximum SSA – minimum SSA.

Atmos. Chem. Phys. Discuss., doi:10.5194/acp-2016-30, 2016
Manuscript under review for journal Atmos. Chem. Phys.
Published: 22 January 2016
© Author(s) 2016. CC-BY 3.0 License.

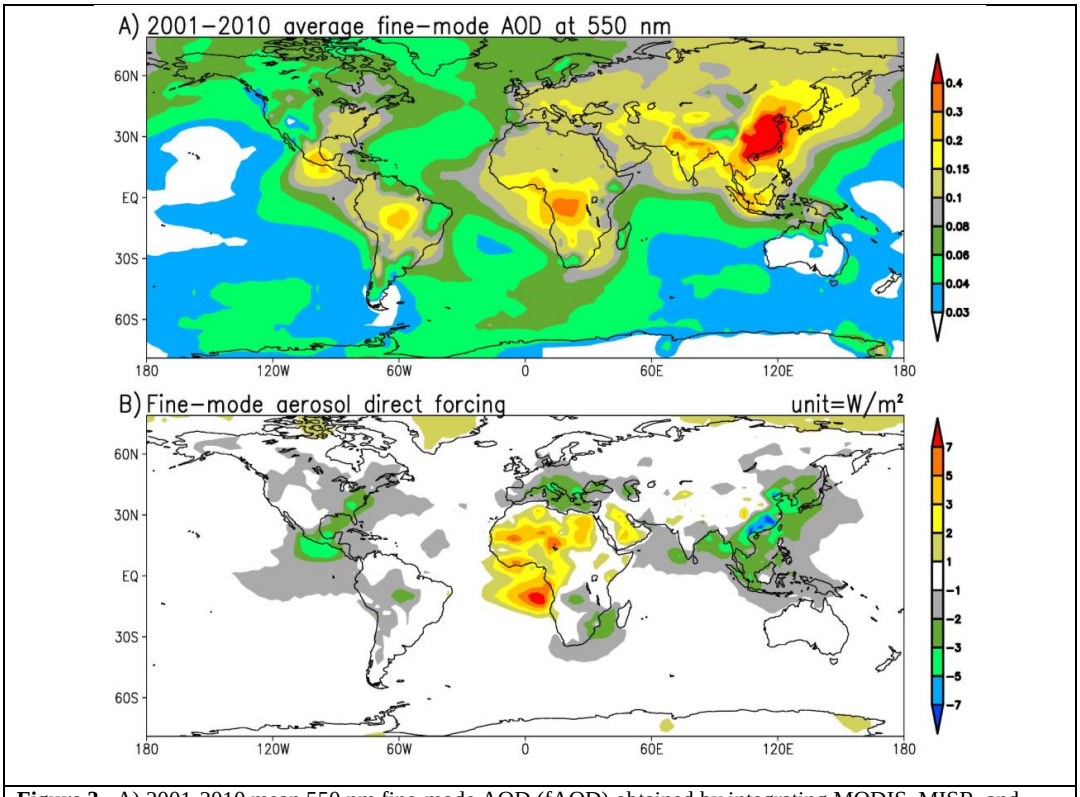

Figure 3. A) 2001-2010 mean 550 nm fine-mode AOD (fAOD) obtained by integrating MODIS, MISR, and AERONET data. B) 2001-2010 mean fine-mode aerosol direct forcing in units of Wm^{-2}; this estimate includes natural fine-mode particles.

Atmos. Chem. Phys. Discuss., doi:10.5194/acp-2016-30, 2016
Manuscript under review for journal Atmos. Chem. Phys.
Published: 22 January 2016
© Author(s) 2016. CC-BY 3.0 License.

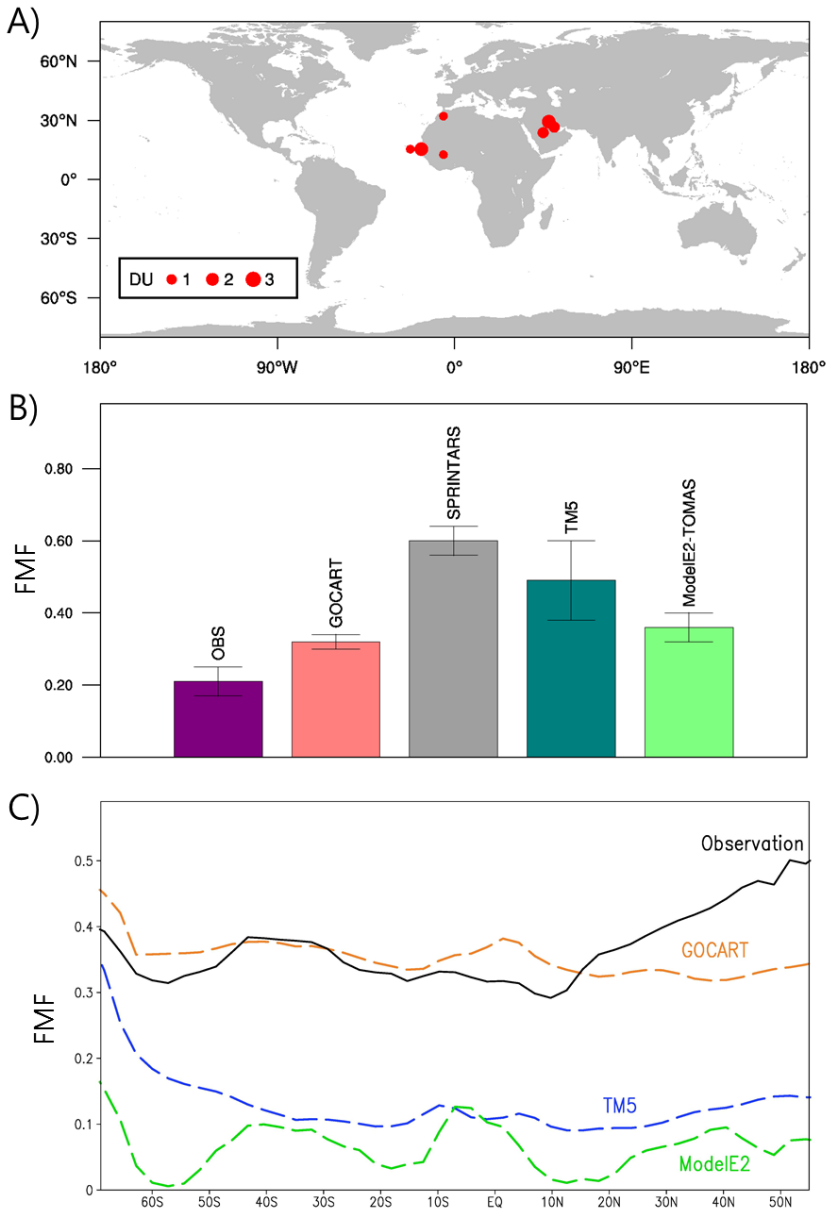

Figure 4. Comparison of simulated and observed fine-mode fraction (FMF) at 550 nm. A) Chosen dust-dominated (DU: red dots) AERONET sites. The dot size is proportional to the number of AERONET climatological data. B) Simulated and observed FMF averaged over the chosen dust dominated sites. FMF averages are made by the average AOD and fAOD. The uncertainty represents ±1.0 standard deviation resulting from variation over the sites. FMFs here include the contribution from non-dust particles. C) Sea salt AOD FMF

Atmos. Chem. Phys. Discuss., doi:10.5194/acp-2016-30, 2016
Manuscript under review for journal Atmos. Chem. Phys.
Published: 22 January 2016
© Author(s) 2016. CC-BY 3.0 License.

Atmospheric Chemistry and Physics Discussions

along the 180th meridian (180° longitude), using annual average AODs. For observation, total FMF (instead of sea salt AOD FMF) is displayed.

Atmos. Chem. Phys. Discuss., doi:10.5194/acp-2016-30, 2016
Manuscript under review for journal Atmos. Chem. Phys.
Published: 22 January 2016
© Author(s) 2016. CC-BY 3.0 License.

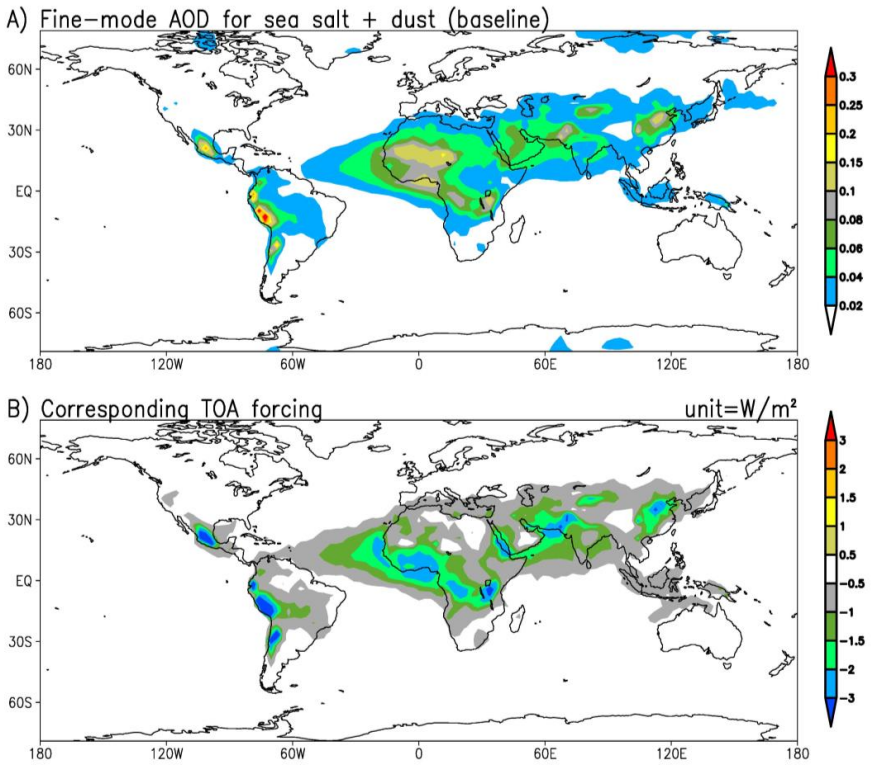

Figure 5. A) 2001-2010 mean fine-mode AOD at 550 nm for sea salt and dust, which is calculated as simulated ratio × observational large-mode AOD, where the simulated ratio refers to $\frac{\text{Model−mix fine−mode AOD for sea salt and dust}}{\text{Model−mix large−mode AOD for sea salt and dust}}$. The observational large-mode AOD is computed by integrating AERONET, MODIS and MISR data. Model mix is an optimal mixture of GOCART, TM5 and ModelE2-TOMOS AOD simulations. B) Aerosol direct radiative effect due to the sea salt and dust fine mode aerosols.

Atmos. Chem. Phys. Discuss., doi:10.5194/acp-2016-30, 2016
Manuscript under review for journal Atmos. Chem. Phys.
Published: 22 January 2016
© Author(s) 2016. CC-BY 3.0 License.

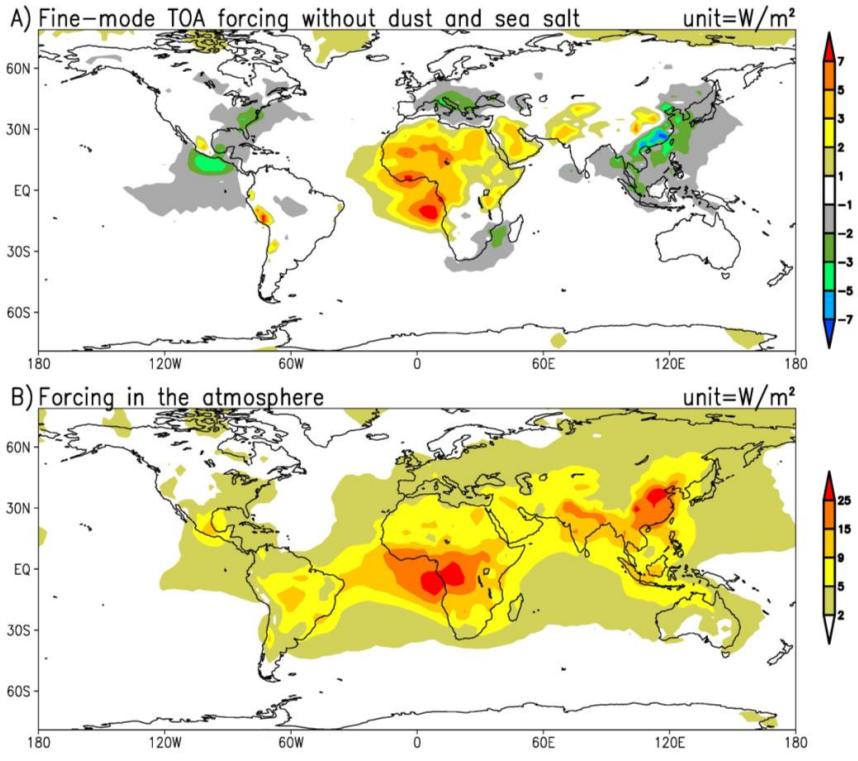

Figure 6. Fine-mode aerosol direct forcing without dust and sea salt in units of Wm^{-2} (baseline). A) TOA forcing. B) Atmospheric forcing.